Tectonophysics 482 (2010) 3–15

Contents lists available at ScienceDirect

Tectonophysics

journal homepage: www.elsevier.com/locate/tecto

Global crustal stress pattern based on the World Stress Map database release 2008

Oliver Heidbach [a,b,c,*], Mark Tingay [d], Andreas Barth [a,b], John Reinecker [e], Daniel Kurfeß [a,b], Birgit Müller [a,b]

[a] Geophysical Institute, University of Karlsruhe, Hertzstr.16, 76187 Karlsruhe, Germany
[b] Heidelberg Academy of Sciences and Humanities, Karlstr.4, 69117 Heidelberg, Germany
[c] GFZ German Research Centre for Geosciences, Telegrafenberg, 14473 Potsdam, Germany
[d] Department of Applied Geology, Curtin University, Perth 6845, Australia
[e] Institute for Geosciences, University of Tübingen, Sigwartstr.10, 72074 Tübingen, Germany

ARTICLE INFO

Article history:
Received 30 September 2008
Received in revised form 20 July 2009
Accepted 28 July 2009
Available online 4 August 2009

Keywords:
Global tectonics
Stress pattern
Tectonic stress
Stress indicators
Database

ABSTRACT

The World Stress Map (WSM) project is a global compilation of information on the contemporary crustal stress field from a wide range of stress indicators. The WSM database release 2008 contains 21,750 stress data records that are quality-ranked using an updated and refined quality-ranking scheme. Almost 17,000 of these data records have A–C quality and are considered to record the orientation of maximum horizontal compressional stress S_H to within ±25°. As this is almost a triplication of data records compared with the first WSM database release in 1992, we reinvestigate the spatial wave-length of the stress patterns with a statistical analysis on a global 0.5° grid. The resulting smoothed global stress map displays both; the mean S_H orientation that follows from the maximum smoothing radius for which the standard deviation is <25° and a countour map that displays the wave-length of the stress pattern. This smoothed global map confirms that long wave-length stress patterns (>2000 km) exist for example in North America and NE Asia. These have been used in earlier analyses to conclude that the global stress pattern is primarily controlled by plate boundary forces that are transmitted into the intraplate region. However, our analysis reveals that rather short wave-length of the stress pattern <200 km are quite frequent too, particularly in western Europe, Alaska and the Aleutians, the southern Rocky Mountains, Basin and Range province, Scandinavia, Caucasus, most of the Himalayas and Indonesia. This implies that local stress sources such as density contrasts and active fault systems in some areas have high impact in comparison to plate boundary forces and control the regional stress pattern.

1. Introduction

The first public release of the World Stress Map (WSM) database in 1992 revealed that long spatial wave-length stress patterns (>2000 km) exist in many plates, such as North America, Europe and South America (Zoback et al., 1989; Richardson, 1992; Zoback, 1992). Furthermore, the contemporary orientation of the maximum horizontal compressional stress S_H was primarily oriented sub-parallel to absolute plate motion in large areas of North America, Western Europe and South America (Zoback et al., 1989; Gregersen, 1992; Richardson, 1992; Zoback, 1992). This suggested that the plate boundary forces that drive plate motion, such as ridge push and slab pull, also have a first-order control on the intraplate stress pattern (Zoback et al., 1989; Richardson, 1992; Zoback, 1992).

The initial WSM database release 1992, in addition to subsequent regional stress studies, also demonstrated that second-order stress patterns with spatial wave-lengths of ~500 km can be caused by lithospheric flexure and intraplate lateral density contrasts, such as continental rifting, isostatic compensation, topography, and deglaciation (Gregersen and Basham, 1989; Zoback, 1992; Coblentz and Sandiford, 1994; Coblentz et al., 1998; Hillis and Reynolds, 2000; Zoback and Mooney, 2003; Dyksterhuis et al., 2005; Bird et al., 2006).

Since the first WSM database release in 1992, there has been an increase of the WSM database from ~7700 to 21,750 data records in 2008 (Heidbach et al., 2008, 2009). Almost 17,000 of these data records have A–C quality and are considered to record the S_H orientation to within ±25° (Fig. 1). The last ten years have also witnessed a major increase in the amount of closely spaced stress data from numerous sedimentary basins that allows a more detailed examination of 'third-order' stress patterns on a 1–100 km scale (Tingay et al., 2005a,b, 2006; Heidbach et al., 2007). Third-order stress patterns can be generated by local density and strength contrasts, basal detachment, basin geometry, topography and active faulting (Bell, 1996; Müller et al., 1997; Tingay et al., 2005a,b, 2006; Heidbach et al., 2007).

The substantially smaller WSM database available in 1992 resulted in third-order stress patterns typically being either not observed or smoothed out and ignored (Heidbach et al., 2007). For example,

* Corresponding author. GFZ German Research Centre for Geosciences, Telegrafenberg, 14473 Potsdam, Germany. Tel.: +49 331 288 2814; fax: +49 331 288 1227.
E-mail address: heidbach@gfz-potsdam.de (O. Heidbach).

0040-1951/$ – see front matter © 2009 Elsevier B.V. All rights reserved.
doi:10.1016/j.tecto.2009.07.023

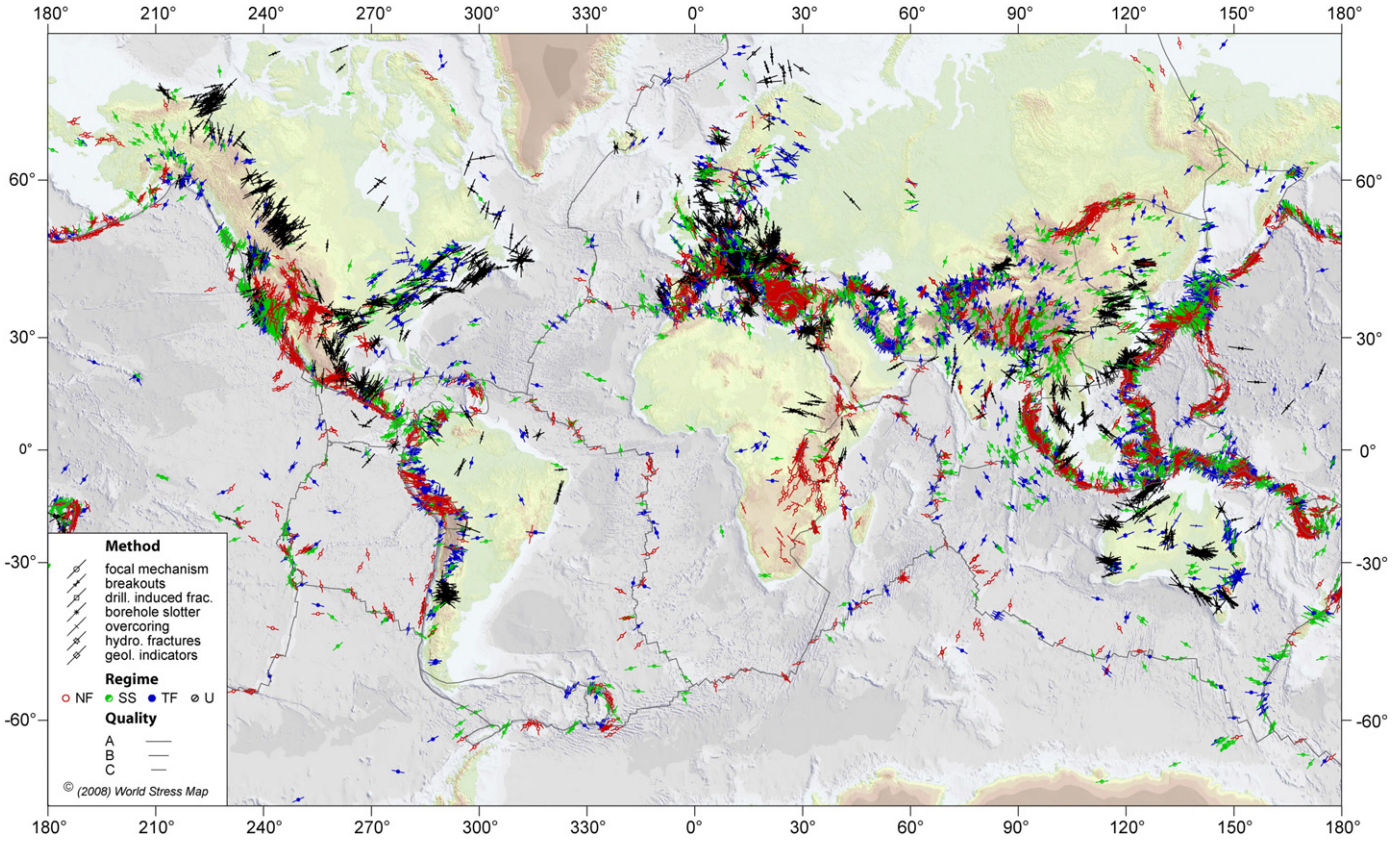

Fig. 1. Global stress map based on the WSM database release 2008 using the 11,346 stress data records with of A–C quality, but excluding all Possible plate Boundary Events (PBE) (Heidbach et al., 2008, 2009). Lines represent orientations of maximum horizontal compressional stress S_H, line length is proportional to quality. Colours indicate stress regimes with red for normal faulting (NF), green for strike-slip faulting (SS), blue for thrust faulting (TF), and black for unknown regime (U). Plate boundaries are taken from the global model PB2002 of Bird (2003). Topography is based on the ETOPO1 data from the National Geophysical Data Center (NGDC) including bathymetry data from Smith and Sandwell (1997).

Müller et al. (2010-this issue) discuss in detail the stress pattern and stress sources in Romania. They note that earlier stress analysis in Romania overly smoothed this stress data (Bada et al., 1998) using a smoothing radius of >100 km to provide a regional stress pattern. However, the smoothed stress field has a mean deviation of >40° from the observed S_H orientation and thus is an inappropriate representation of the stress pattern. Furthermore, the mean S_H orientation of the WSM data records in Romania is N70°, but with a standard deviation of 59.5° (Müller et al., 2010-this issue). Both values indicate that there is no regional trend in the stress pattern of Romania, but that the S_H orientation varies on local scale, and thus is controlled by local stress sources.

The widespread occurrence of localised stress patterns has been postulated in the first global statistical stress pattern analysis conducted by Coblentz and Richardson (1995). Their study investigated the spatial wave-length of the stress pattern by estimating the mean S_H orientation for 5°×5° bins using a subset with 4527 A–C quality stress data records from the WSM database release 1992. In their statistical analysis Coblentz and Richardson (1995) allowed a maximum standard deviation s_0<25° for the mean S_H orientation in each bin. As a result, they found that in half of the 382 bins that contained two or more stress data records s_0>25° indicating that the stress pattern is probably controlled by regional or local stress sources. The results in the other bins with s_0<25° indicates that broad regions of consistent mean S_H orientation exist. However, their work did not quantify the varying wave-length of the stress pattern, but provides an estimate whether the S_H orientation within a bin is random or not. Their fixed bin size of 5°×5° implies a fixed global search radius of approximately 250 km.

The primary aim of this study is to quantify the global variation of the spatial wave-lengths of the stress pattern and to provide the mean S_H orientation on a global 0.5° grid based on a sound statistical analysis using the extensive WSM database release 2008. We first describe the major achievements and advancements of the WSM project that have resulted in an almost three-fold increase of data records in the WSM database since 1992. We then examine the global stress patterns utilizing this greatly expanded 2008 WSM database. Instead of using 5°×5° bins to estimate the mean S_H orientation (Coblentz and Richardson, 1995), we apply variable search radii on a global 0.5° grid and determine the search radius at which the null hypothesis of random S_H orientations can be rejected. This procedure

Table 1
Data type and data quality in the WSM database release 2008 (Heidbach et al., 2008, 2009).

Data type (abbreviation)	WSM 2008 A–E quality	WSM 2008 A–C quality
Focal mechanisms (FMF, FMS, FMA)	15,689[a]	13,959[b]
Borehole breakouts (BO, BOC, BOT)	4125	2168
Drilling-induced fractures (DIF)	278	82
Geological: fault-slip (GFI, GFM, GFS)	434	331
HydroFrac (HF, HFG, HFP, HFM)	349	228
Borehole slotter (BS)	33	0
Overcoring (OC)	611	94
Geological: volcanic alignment (GVA)	220	98
Petal centreline fractures (PC)	9	9
Shear wave splitting (SW)	2	0
Total	21,750	16,969

[a] This number includes 5669 data records from single focal mechanism solutions (FMS) located close to a plate boundary and flagged as possible plate boundary event (PBE) indicating that they have a larger potential for a large offset between the principal strain axis and the principal stress orientations (further details are given in Section 2.3).
[b] This number includes 5623 data records from single mechanism solutions (FMS) that are flagged as PBE (further details are given in Section 2.3).

Table 2
2008 World Stress Map quality-ranking system for S_H orientation.

Stress indicator		A	B	C	D	E
		S_H believed to be within ±15°	S_H believed to be within ±15–20°	S_H believed to be within ±20–25°	Questionable S_H orientation (±25–40°)	No reliable information (>±40°)
Focal mechanism (FM)	Formal inversion (FMF)	• Formal inversion of ≥15 well constrained single event solutions in close geographic proximity and s.d. or misfit angle ≤12°	• Formal inversion of ≥8 well constrained single event solutions in close geographic proximity and s.d. or misfit angle ≤20°	–	–	–
	Single (FMS)	–	–	• Well constrained single event solution, $M \geq 2.5$ (e.g. CMT solutions)	• Well constrained single event solution, $M < 2.5$	• Mechanism with P,B,T axes all plunging 25°–40°
	Average (FMA)	–	–	–	• Average of P-axis trends or circular statistics of P-axis trends • Composite solutions	• Mechanism with P and T axes both plunging 40°–50°
Borehole breakout (BO)	From caliper logs	• ≥10 distinct breakouts and combined length ≥ 300 m in a single well with s.d. ≤ 12°	• ≥6 distinct breakouts and combined length > 100 m in a single well with s.d. ≤ 20°	• ≥4 distinct breakouts and combined length ≥ 30 m with s.d. ≤ 25°	• <4 distinct breakouts or <30 m combined length in a single well with s.d. ≤ 40°	• Wells without reliable breakouts or s.d. > 40°
	From image logs	• ≥10 distinct breakouts and combined length ≥ 100 m in a single well with s.d. ≤ 12°	• ≥6 distinct breakouts and combined length > 40 m in a single well with s.d. ≤ 20°	• ≥4 distinct breakouts and combined length ≥ 20 m with s.d. ≤ 25°	• <4 distinct breakouts or <20 m combined length in a single well with s.d. ≤ 40°	
Drilling-induced fractures (DIF)		• ≥10 distinct fractures in a single well with a combined length ≥ 100 m and s.d. ≤ 12°	• ≥6 distinct fractures in a single well with a combined length ≥ 40 m and s.d. ≤ 20°	• ≥4 distinct fractures in a single well with a combined length ≥ 20 m and s.d. ≤ 25°	• <4 distinct fractures in a single well or a combined length < 20 m and s.d. ≤ 40°	• Wells without fracture zones or s.d. > 40°
Hydraulic fracture (HF)		• ≥5 hydrofrac orientations in a single well with s.d. ≤ 12° • Depth ≥ 300 m, and distributed over a depth range ≥ 300 m	• ≥4 hydrofrac orientations in a single well with s.d. ≤ 20° • Depth ≥ 100 m, and distributed over a depth range ≥ 200 m	• ≥3 hydrofrac orientations in a single well with s.d. ≤ 25° • Depth ≥ 30 m, and distributed over a depth range ≥ 100 m	• Single hydrofrac orientation	• Wells in which only stress magnitudes are measured, without information on orientations
Overcoring (OC) and borehole slotter (BS)		• ≥11 measurements with depth ≥ 300 m and s.d. ≤ 12°	• ≥8 measurements with depth ≥ 100 m and s.d. ≤ 20°	• ≥5 measurements with depth ≥ 30 m and s.d. ≤ 25°	• ≥2 measurements with depth ≥ 10 m and s.d. ≤ 40°	•<2 measurements or depth < 10 m or s.d. > 40° • Measurements in boreholes extending less than two excavation radii from the excavation wall • Distance to topographic features less than three times the height of the topographic feature
Fault-slip (GF)		• Inversion of ≥25 fault-slip data with a fluctuation ≤9° for ≥60% of the whole dataset	• Inversion of ≥15 fault-slip data with a fluctuation ≤12° for ≥45% of the whole dataset	• Inversion of ≥10 fault-slip data with a fluctuation ≤15° for ≥30% of the whole dataset • Attitude of fault and primary sense of slip known, no actual slip vector	• Inversion of ≥6 fault-slip data with a fluctuation ≤18° for ≥15% of the whole dataset • Offset core holes or quarry popups • Postglacial surface fault offsets	–
Volcanic vent alignment (GVA)		• ≥5 Quaternary vent alignments or "parallel" dikes with s.d. ≤ 12°	• ≥3 Quaternary vent alignments or "parallel" dikes with s.d. ≤ 20°	• Single well-exposed Quaternary dike • Single alignment with ≥5 vents	• Volcanic alignment inferred from <5 vents	–
Petal centerline fractures (PC)		–	–	• Mean orientation of fractures in a single well with s.d. ≤ 20°	–	–

s.d. is standard deviation.

results in the quantification of the appropriate search radius and the mean S_H orientation. As a result, we obtain a smoothed global stress map that displays both, the mean S_H orientation on a 0.5° grid and a contour map illustrating the wave-length of the stress pattern.

2. The WSM database release 2008 — recent achievements and changes

In the following three sections we briefly describe the major changes and recent achievements of the WSM project, particularly the updated and refined quality-ranking scheme for the S_H orientation.

2.1. Database overview

The WSM database release 2008 contains 21,750 data records (Heidbach et al., 2008, 2009), and approximately 17,000 A–C quality S_H orientations, determined from a wide range of stress indicators (Table 1). The present-day S_H orientation is primarily estimated from earthquake focal mechanism solutions, borehole breakouts and drilling-induced fractures (from borehole images or caliper log data), in-situ stress measurements (overcoring, hydraulic fracturing) and geological indicators (fault-slip data, volcanic vent alignments). The informations from the different stress indicators represent various crustal rock volumes ranging from 10^{-3} to $10^{9}\,m^3$ (Ljunggren et al., 2003) and depths ranging from near the surface down to 40 km. Within the upper 6 km of the Earth's crust the stress field is mapped by a wide range of methods with borehole breakouts as the major contributor. Below ~6 km depth earthquake focal mechanisms are the only stress indicators available, except from a few scientific drilling projects. Furthermore, the WSM project website now provides easy to use guidelines for the analysis and quality assessment of present-day S_H orientations from earthquake focal mechanism solutions, borehole breakouts, drilling-induced tensile fractures and overcoring tests (http://www.world-stress-map.org).

2.2. Quality-ranking scheme

A critical factor of the WSM project is the quality-ranking of all stress indicators following an internationally developed scheme. This quality-ranking scheme provides an assessment of the reliability of each individual stress indicator and also facilitates comparison between S_H orientations that are obtained using different measurement techniques and observed at different depths (Zoback and Zoback, 1989, 1991; Zoback, 1992; Sperner et al., 2003). Each stress data record is assigned a quality between A and E, with A being the highest quality and E the lowest. A-quality indicates that the S_H orientation is accurate to within ±15°, B-quality to within ±20°, C-quality to within ±25°, and D-quality to within ±40°. E-quality marks data records with insufficient or widely scattered stress information. Data records assigned to A-, B-, or C-quality are typically considered reliable for use in stress analysis and the interpretation of geodynamic processes (Zoback and Zoback, 1989, 1991; Zoback, 1992; Sperner et al., 2003). The quality-ranking scheme has been refined and extended as existing techniques were further developed (Zoback and Zoback, 1989, 1991; Zoback, 1992; Sperner et al., 2003). These changes are described in the following sections.

2.2.1. Quality-ranking scheme for borehole breakouts

The original 1992 WSM quality-ranking scheme for stress data from borehole breakouts required only four breakouts or a total of at least 30 m of breakouts (often in multiple nearby wells) with a standard deviation of <25° to be rated as C-quality. However, at this time borehole breakouts were primarily interpreted from four-arm caliper logs, on which non-stress related features can easily be misinterpreted as breakouts (a problem that is particularly common with automatic breakout interpretation software). Furthermore, four breakouts or ≥30 m of breakout can encompass a very small volume of rock and the use of wells in 'close proximity' was ambiguous (sometimes interpreted to be all wells within the same basin). Hence, this quality-ranking scheme overestimated the reliability of borehole breakout in some areas for assessing the regional stress pattern. Because of these flaws, Sperner et al. (2003) introduced a refined quality-ranking system for stress data from borehole breakouts in which both four breakouts and a combined length of ≥30 m must be met in a single well to obtain a C-quality. Furthermore, all breakouts interpreted using automatic software (i.e. not manually picked and identified) were disallowed and removed from the database.

The last decade has also witnessed the more prevalent use of electric and acoustic image logs that allow borehole breakouts to be directly visualised and thus remove much of the possibility for misinterpretation. Image logs also allow the interpretation of much smaller breakouts (e.g. tens of cm rather than >1 m for caliper logs) and of drilling-induced fractures, that were too small to be interpreted on caliper logs. Hence, image logs enable a much more accurate and improved interpretation of stress orientation over four-arm caliper logs. However, the greater reliability of stress orientations interpreted from image log data was underestimated under the Sperner et al. (2003) quality-ranking scheme. For example, the common image log observation of numerous small consistently-oriented breakouts over a long image log interval (e.g. 25 one meter log breakouts over several hundred meters of log) would only receive a D-quality under the quality-ranking scheme described in Sperner et al. (2003), despite reliably reflecting the S_H orientation in a significant volume of rock. Hence, the WSM database release 2008 now includes different quality-ranking schemes for breakouts interpreted on four-arm caliper logs and for breakouts interpreted on image logs and a quality-ranking scheme for drilling-induced fractures that better reflects the ability for different log types to reliably estimate the contemporary S_H orientation (Table 2).

2.2.2. Quality-ranking scheme for focal mechanism solutions

The majority of earthquake focal mechanism solutions in the WSM database are derived from single seismic events (denoted as FMS). Due to the expansion of the global seismic network and regional broadband networks the number and quality of earthquake focal mechanism solutions increased significantly in the last decade. Furthermore, new techniques have been developed that allow to determining focal mechanism solutions for earthquakes with smaller magnitudes (e.g. Barth et al., 2007). This significant increase of earthquake focal mechanism solutions allows the application of formal stress inversion techniques in which a large number of single event solutions are used to better estimate the principal stress orientations and relative stress magnitudes (e.g.; Hardebeck and Michael, 2004; Kastrup et al., 2004; Townend and Zoback, 2004; Townend and Zoback, 2006; Barth et al., 2007; Barth and Wenzel, 2010-this issue). The most common inversion techniques were developed by Angelier (1979), Michael (1984), Gephart and Forsyth (1984), and Rivera and Cisternas (1990).

In order to account for this development, we refined and restructured the WSM quality-ranking scheme for focal mechanism

Fig. 2. Histogram of the lesser of the two deviations between the nodal plane azimuths of single focal mechanism solutions and the plate boundary azimuth. First column gives the deviation distribution of all stress data records deduced single focal mechanism solutions with the appropriate tectonic regime (SS = strike-slip, TS = transpression, NS = transtension, TF = thrust faulting, NF = normal faulting). Second column shows the deviation distribution for the datasets within the critical distance d_{crit} that resulted from the statistical analysis of the deviation distribution and the third column the deviation distribution for datasets beyond the critical distance. Rows show the deviation distribution for the different plate boundary types.

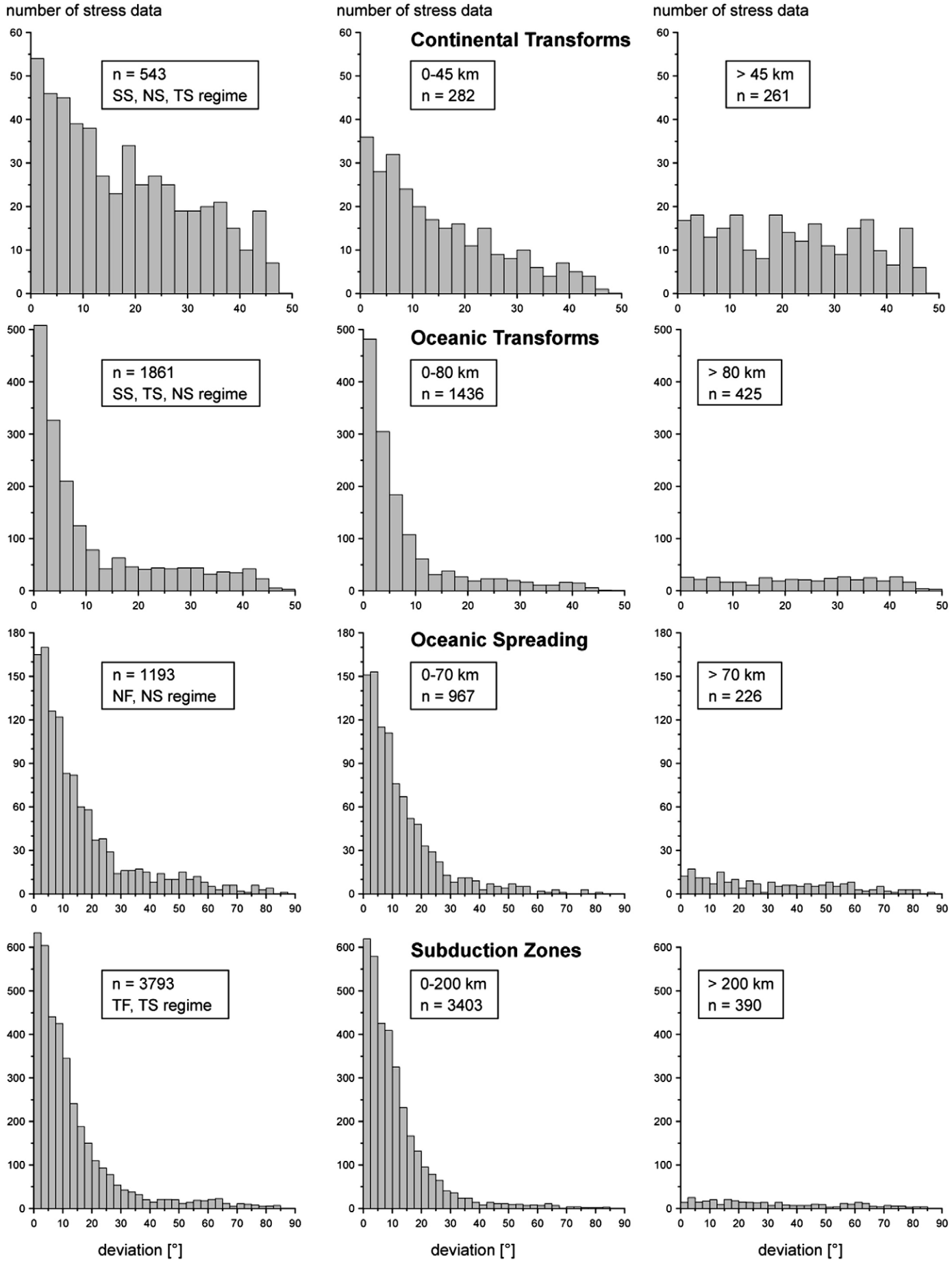
number of stress data
n = 543
SS, NS, TS regime
Continental Transforms
0-45 km
n = 282
> 45 km
n = 261
n = 1861
SS, TS, NS regime
Oceanic Transforms
0-80 km
n = 1436
> 80 km
n = 425
n = 1193
NF, NS regime
Oceanic Spreading
0-70 km
n = 967
> 70 km
n = 226
n = 3793
TF, TS regime
Subduction Zones
0-200 km
n = 3403
> 200 km
n = 390
deviation [°]

solutions (FM*) and added the new subtype FMF for stress data records from formal stress inversions. Since formal inversions minimise the difference between earthquake slip direction and maximum shear stress (Wallace–Bott hypothesis, Bott, 1959) the result of the inversion gives a standard deviation or average misfit angle from the minimization procedure. We use this misfit angle and the number of focal mechanisms used for the inversion to quality-rank the resulting S_H orientation (Table 2).

The quality of a formal inversion cannot be inferior than B-quality ($\pm 20°$). A higher average misfit angle or standard deviation would be in conflict with the C-quality ($\pm 25°$) that is per default assigned to all data records from FMS data (Table 2). If the result of a formal inversion is not better than the quality resulting from single focal mechanism solutions one has to assume that either the binning is not appropriate (i.e. the assumption made for the formal inversion that all events in a bin are driven by the same stress tensor is violated) or that the quality of the incorporated focal mechanism solutions is poor.

Furthermore, we restructured the original average focal mechanism solution (FMA) data type that formerly included formal inversions. This FMA data type now consists of stress data records from averaged or composite focal mechanisms only. Since these two methods do not take into account the conceptual difference between the stress tensor and the moment tensor they might be even less precise in fault plane orientations than FMS and thus are now all assigned to D-quality (reliable within $\pm 40°$).

2.3. Possible Plate Boundary Events (PBE)

The advantage of using well constrained single focal mechanisms solutions is that they record stress induced deformation at depths where no other stress indicator is available and that they provide reliable information on the relative magnitudes of the principal stresses from which the tectonic regime can be determined. Nevertheless, a critical issue utilizing single focal mechanism solutions as stress indicators is that the P-, B-, and T-axis of the moment tensor do not necessarily coincide with the principal stress directions. In particular McKenzie (1969) showed that for the general case the only theoretical restriction on the maximum principal stress orientation is that it lies in the same quadrant as the P-axis. Despite this, Raleigh et al. (1972) state that the typical strength of homogeneous rock is such that new fractures are more likely to be generated than the reactivation of non-optimal oriented pre-existing faults. However, there is also evidence that non-optimally oriented faults may be preferentially reactivated if they have a very low coefficient of friction (Hickman, 1991; Bird and Kong, 1994; Streit, 1997; Zoback, 2000). Hence, the possible discrepancy between the P-, B-, and T-axis that are taken as proxies for the principal stress orientation, and the true orientation of the principal stress largely depends on the coefficient of friction of existing faults (McKenzie, 1969; Raleigh et al., 1972; Zoback and Healy, 1984).

Due to these limitations a single focal mechanism solution is never assigned better than a C-quality in the WSM database (i.e. showing the S_H orientation to within $\pm 25°$). However, plate boundaries are likely to be zones of mechanical weakness that are potentially not optimally oriented with respect to the stress field. This is sufficient grounds for doubting and critically assessing the reliability of S_H orientations deduced from single focal mechanism solutions that are located near presumably weak plate boundary zones.

In the current WSM database release 2008 we flag stress data records from single focal mechanism solutions as possible 'Plate Boundary Events' (PBE) when they meet the following three criteria. (1) The tectonic regime of the single focal mechanism solution reflects the plate boundary kinematics. (2) One of the two deviations between the azimuth of the two nodal planes and the azimuth of the plate boundary is <30°. (3) The event is located within the plate boundary zone of width *w*.

The first two criteria can be checked using the tectonic regime that results from the focal mechanism solutions and the *a priori* chosen value of 30° for deviation between the azimuth of the two nodal planes and the azimuth of the plate boundary. For the third criterion, the width *w* of the plate boundary zone needs to be defined. Assuming that faults within plate boundary zones have a prevailing orientation that is similar to the major fault that defines the plate boundary, one of the deviations between the two nodal plane azimuths and the plate boundary azimuth is expected to be small. Thus, the histogram of the lesser of the two deviations should have a normal distribution (Fig. 2, second column). Outside the plate boundary zone of width *w* the distribution of the deviation is expected to be uniform (Fig. 2, third column). To test the null hypothesis that outside the plate boundary width *w* the distribution of the lesser of the two deviations is uniform we perform a chi-squared test of goodness of fit on a 99.5% confidence probability.

The subset used for this statistical analysis consists of 14,158 stress data records of the WSM database release 2008 that are deduced from single focal mechanism solutions. We first estimate for each data record of this subset the distance to the closest plate boundary segment using the global plate model PB2002 from Bird (2003). The plate boundary length of 260,000 km is divided into 5819 segments with a length between 1 and 109 km and each segment is assigned to one of the seven different plate boundary types stated in the PB2002 model: continental transform faults, oceanic transform faults, oceanic spreading ridges, subduction, continental collision boundary, oceanic collision boundary, and continental rifting boundary.

In a second step we group the stress data records from single focal mechanism solutions into seven subsets according to the closest plate boundary type that has been assigned to the event and take off all data records that do not have the appropriate tectonic regime (Table 3). The lesser of the two deviations between the two nodal plane azimuths and the plate boundary azimuth is binned into ten classes of five degrees for oceanic and continental transforms (CTF and OTF), ranging from 0–50° and into 18 classes of five degrees for the other five plate boundary types, thus ranging from 0–90°. The bin size ensures that each class has a sufficient number of data for a reasonable statistical analysis. We then perform the chi-square goodness-of-fit test for binned data on a 99.5 % confidence probability for the data that are at a critical distance d_{crit} to the nearest plate boundary.

The d_{crit} is then increased from zero in steps of 5 km until our null hypothesis of a uniform deviation distribution is accepted (Fig. 2, third column). When the value of the chi-square goodness-of-fit test reaches the test statistic (23.59 for 10 classes and 35.72 for 18 classes at the 99.5 % confidence probability), we find that d_{crit} is 45 km for continental transform faults, 80 km for oceanic transform faults, 70 km for oceanic spreading ridges, and 200 km for subduction zones

Table 3
Subsets of A–C quality focal mechanism solutions (FMS) according to their tectonic regime and the type of the nearest plate boundary.

Plate boundary type[a]	Tectonic regime	n[b]	d_{crit} [km]	$d<d_{crit}$[c] [km]	PBE[d]	Percentage[e]
Continental transform	SS, TS, NS	543	45	282	245	87
Oceanic transform	SS, TS, NS	1861	80	1436	1359	95
Oceanic spreading ridge	NF, NS	1193	70	967	881	91
Subduction	TF, TS	3793	200	3403	3184	94
Continental collision	TF, TS	881	–	–	–	–
Oceanic collision	TF, TS	197	–	–	–	–
Continental rifting	NF, NS	282	–	–	–	–
Sum		8750		6088	5669	93

[a] Plate boundary characterization adapted from the global plate model PB2002 (Bird, 2003).
[b] Number of FMS data records with the suitable tectonic regime.
[c] Number of FMS data records within the critical distances d_{crit}.
[d] Number of FMS data records detected as Possible plate Boundary Events (PBE).
[e] Percentage of PBE.

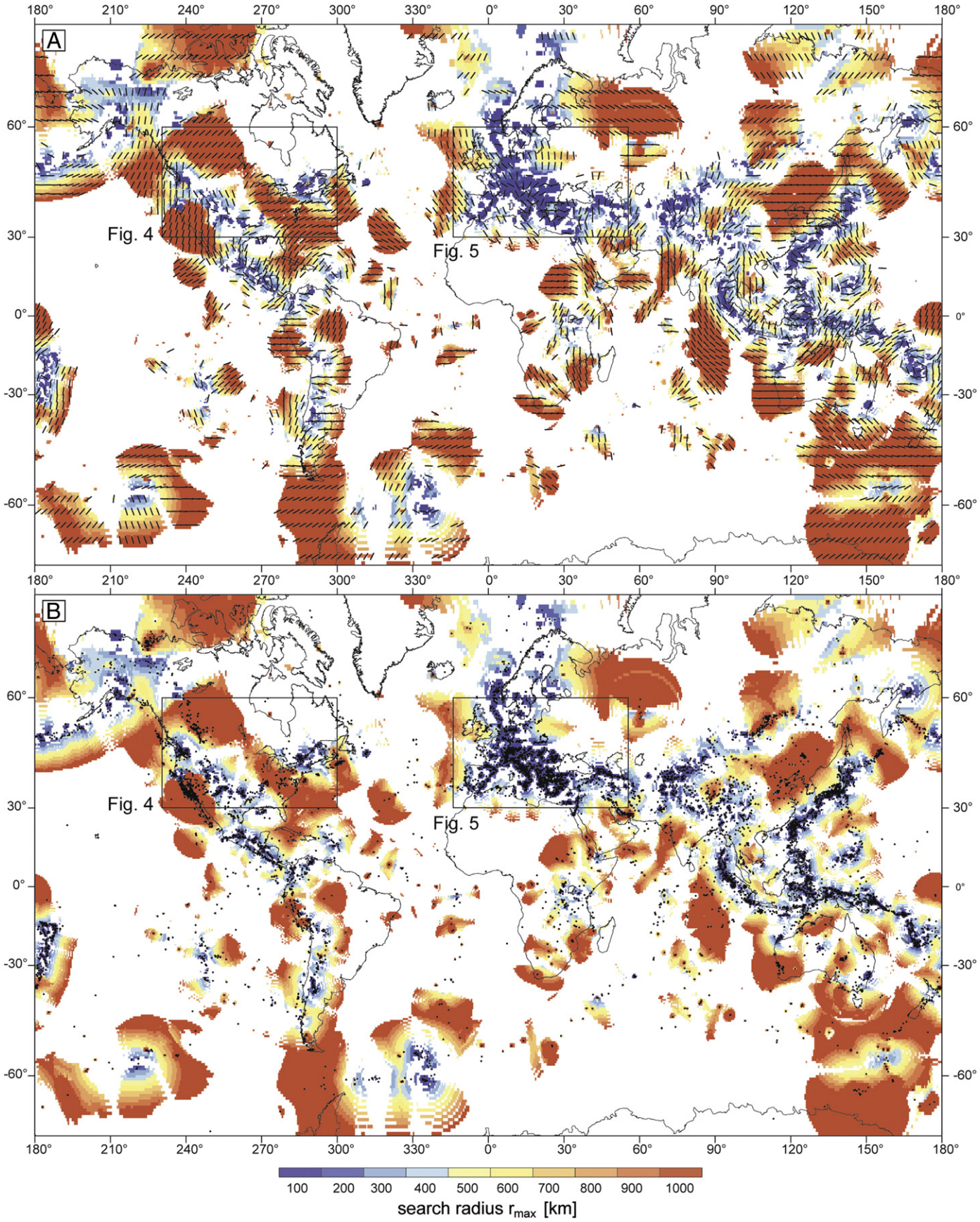

Fig. 3. Results of the statistical stress pattern analysis displayed on global maps. Rectangles indicate the location of Figs. 4 and 5. (A) Global smoothed stress map that displays both; $\hat{S}_H$, the mean orientation of the maximum horizontal compressional stress S_H, and r_{max}, the maximum search radius for which the standard deviation s_0 of the $\hat{S}_H$ orientation $\leq 25^\circ$ (grey lines). Note that a grid point is only plotted when the number of data records N within r_{max} is ≥ 5. (B) Points indicate the locations of the 11,346 A–C quality data records from the WSM database release 2008 as displayed in Fig. 1.

(Table 3). For continental collision the null hypothesis of uniform deviation distribution is not fulfilled for any distance and for oceanic collision and continental rifting boundaries the number of data is insufficient for a sound statistical analysis (Table 3).

From the total number of 14,158 stress data records from single focal mechanism solutions 8750 match the first criterion, i.e. they have the same tectonic regime as their closest plate boundary segment. 6088 of these stress data records are within the statistically determined width of the plate boundary zone. Finally, for 5669 of these data records (93%), the lesser of the two deviations between the plate boundary azimuth and the two nodal plane azimuths is <30° and they thus receive a PBE flag (Table 3).

The default setting in the web-based WSM database interface CASMO (Heidbach et al., 2004) is that PBE are excluded from the visualization of the data on a stress map. However, users can define their own selection criteria for data records that are from single focal mechanism solutions based on the distance to the nearest plate boundary, the plate boundary type, and the tectonic regime of the event. This WSM database interface is available at http://www.world-stress-map.org/casmo.

3. Global wave-length analysis of the stress pattern

We conducted a global spatial wave-length analysis of the stress pattern using a subset of the WSM database release 2008 that contains A–C quality data and excluding the PBE-flagged data records from single focal mechanism solutions. This results in a dataset with 11,347 stress data records which is two and a half times the number of data than used in the statistical analysis of Coblentz and Richardson (1995) and in the purely qualitative analysis of Zoback (1992).

3.1. Analysis procedure

We calculate for a global 0.5° grid $\hat{S}_H$, the mean S_H orientation and s_0, the standard deviation of $\hat{S}_H$. For the determination of the $\hat{S}_H$ orientation, the S_H orientations are weighted by their quality and distance to the grid point. We start with a search radius of 1000 km that is then decreased in steps of 100 km until the search radius r_{max} is reached for which s_0<25°. However, we only plot the $\hat{S}_H$ orientation when at least five data records are within r_{max}. The resulting smoothed global stress map displays both; the $\hat{S}_H$ orientation and the colour-coded r_{max}-values that indicate the wave-length of the stress pattern (twice the search radius) (Fig. 3).

For the computation of the $\hat{S}_H$ orientations the S_H orientations are weighted by their quality (w_Q = 1/15 for A-, w_Q = 1/20 for B-, and w_Q = 1/25 for C-quality data) and their inverse distance to the grid point (w_D = min(1/D, 1/20 km), where D is the distance between the data location and the grid point . The minimum value of w_D = 20 km for the distance weight is necessary in order to avoid an over-representation of data records that are located close to the grid point during calculation of the $\hat{S}_H$ orientation.

According to Mardia (1972) $\hat{S}_H$, the weighted mean of the S_H orientations and s_0, the standard deviation of the $\hat{S}_H$ orientation are defined as:

$$\hat{S}_H = \frac{\arctan 2(\bar{S}, \bar{C})}{2} \bmod 180^\circ \quad (1)$$

$$s_0 = \frac{\sqrt{-2\log_e \bar{R}}}{2} \cdot \frac{180^\circ}{\pi} \quad (2)$$

with

$$\bar{R} = \sqrt{\bar{C}^2 + \bar{S}^2} \quad (3)$$

$$\bar{C} = \frac{1}{Z}\sum_{i=1}^{N} w_i \cos 2\theta_i \quad (4)$$

$$\bar{S} = \frac{1}{Z}\sum_{i=1}^{N} w_i \sin 2\theta_i \quad (5)$$

$$Z = \sum_{i=1}^{N} w_i \quad (6)$$

$$w_i = w_Q w_D. \quad (7)$$

The standard deviation s_0 = 25° corresponds to the mean resultant length $\bar{R}$ = 0.7, which is the value used by Coblentz and Richardson (1995) to discriminate between small and large dispersion of the S_H orientations within their 5°×5° bins.

For our global 0.5° grid the wave-length of the stress pattern is defined by the r_{max}-value for which s_0<25°. Furthermore we demand that within r_{max} the number of data records is $N \geq 5$. If for a grid point none of the tested search radii has s_0<25°, we define "< 100 km" to be its wave-length, but again only if five or more data records are located within the 100 km search radius.

3.2. Results

The results of this statistical analysis are presented with a smoothed global stress map that displays both; the $\hat{S}_H$ orientations that result from r_{max} with s_0<25° and the colour-coded r_{max}-values (Fig. 3). Blue colours indicate that the stress pattern is of regional to local wave-length (second- to third-order; $r_{max} \leq 400$ km); yellow to red colours indicate regional to plate-wide wave-length (first- to second-order, r_{max}>400 km). Qualitatively the results are very similar to the principal findings of Coblentz and Richardson (1995). Large areas show long wave-length stress patterns, such as in North America and NE Asia (Fig. 3). Short wave-length stress patterns prevail in a variety of areas, particularly in the Basin and Range area, central South America, Western Europe, the Caucasus region, Himalaya region, and SE Asia (Fig. 3). Also the $\hat{S}_H$ orientations presented on a 2.5° global grid in Fig. 3A show a very similar pattern to that presented in Coblentz and Richardson (1995) and qualitatively discussed by Zoback (1992) and Zoback and Zoback (1980, 1989, 1991).

Shorter wave-lengths of the stress pattern correlate well with topography (Alps, Andes, Basin and Range, Caucasus, and Himalayas) and with plate boundary zones where the style of plate boundary type varies (Central America, Mediterranean, and SE Asia). There seems to be a correlation between data density and short wave-length of the stress pattern. However, there are also areas with long wave-length where data density is high (California, NW and SE of North America, NE Asia). The coincidence of data density and short wave-lengths is probably simply due to the higher disposability of stress data in tectonically active regions and, at the same time, that these areas have scattered S_H orientations due to intraplate stress sources such as topography, density contrasts, and strength anisotropies. The widespread occurrence of $\hat{S}_H$ rotations on short spatial scales indicates that second- and third-order sources of stress have a major impact on the stress pattern in these regions.

Fig. 4. Smoothed stress map of North America for three different values of s_0; same legend as in Fig. 3A. For all three results the overall pattern of the wave-length remains. The Basin and Range area and the NW coast exhibits short wave-length of their stress pattern. In California the high variability of data density leads to a flip of the colours from blue to red when s_0 is increased. Note that the change of the $\hat{S}_H$ orientation with changing s_0 is insignificant.

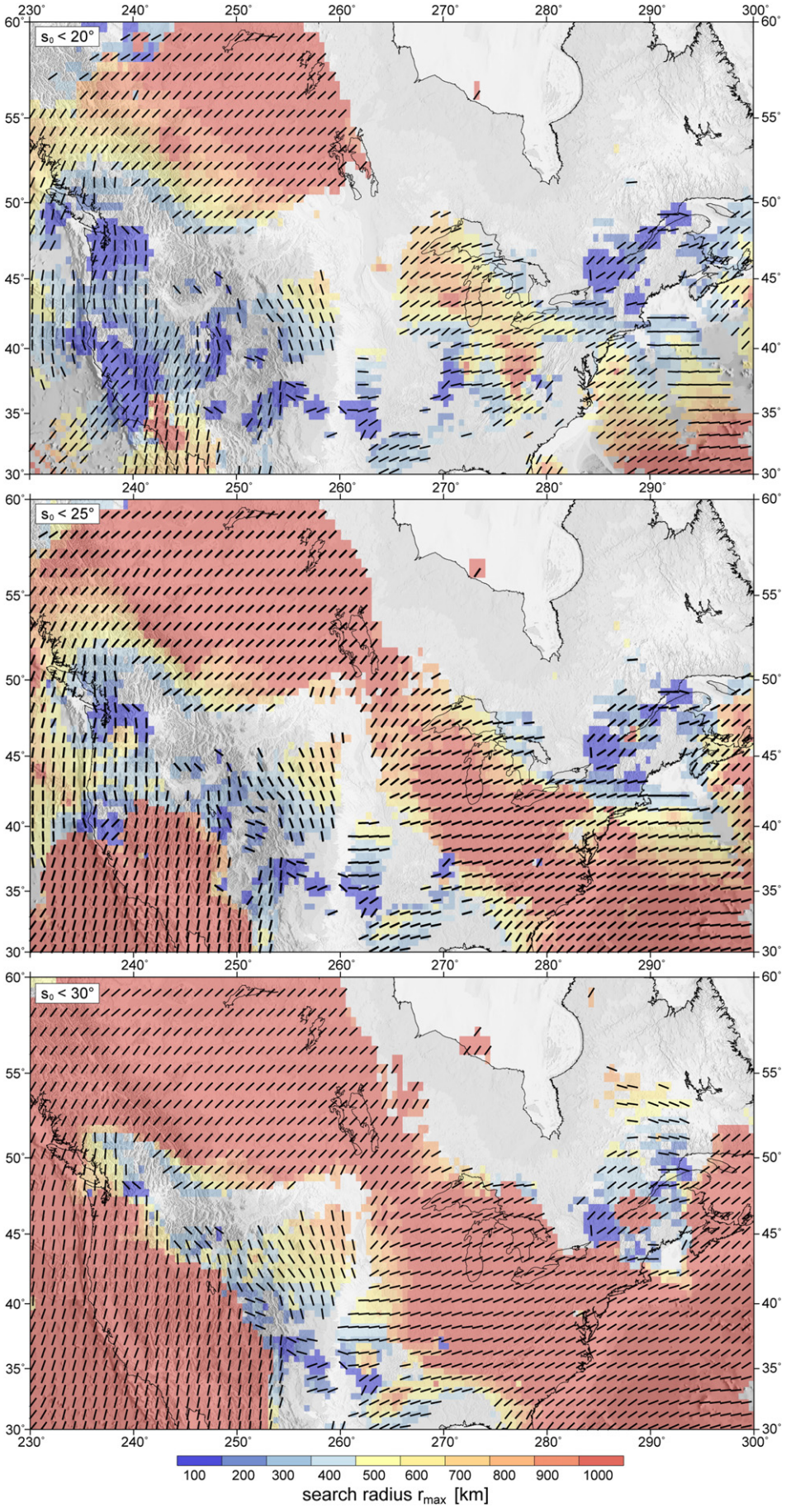
s0 < 20°
s0 < 25°
s0 < 30°
230° 240° 250° 260° 270° 280° 290° 300°
60° 55° 50° 45° 40° 35° 30°
100 200 300 400 500 600 700 800 900 1000
search radius rmax [km]

Table 4
Details on the results of the statistical analysis at four locations.

r	South California 34.25°N, 116.75°W			North California 39.25°N, 120.25°W			South Germany 49.75°N, 9.75°E			Northern Ural 63.25°N, 60.25°W		
	$\hat{S}_H$	s_0	N	$\hat{S}_H$	s_0	N	$\hat{S}_H$	s_0	N	$\hat{S}_H$	s_0	N
10	4.8	6.4	7	14.0	0	1	130.0	0	1	–	–	0
25	0.1	6.9	25	14.0	0	1	128.5	1.5	2	–	–	0
50	5.3	18.3	97	14.9	1.4	2	137.1	11.6	4	–	–	0
100	8.0	18.2	187	10.6	9.5	5	140.9	14.8	13	–	–	0
200	8.1	17.6	335	12.6	23.2	25	145.5	22.1	89	–	–	0
300	8.4	18.1	483	21.6	27.9	78	154.5	26.8	275	–	–	0
400	8.9	18.5	547	23.6	26.5	157	153.5	29.5	419	–	–	0
500	9.0	18.8	595	18.8	25.0	319	153.7	31.1	539	120.0	14.7	3
600	9.1	18.9	621	18.2	24.1	429	153.6	32.7	665	122.3	14.9	5
700	9.2	19.0	649	16.5	23.1	610	154.3	33.7	794	122.3	14.9	5
800	9.2	19.0	677	15.0	23.3	710	153.7	33.9	944	115.2	20.0	7
900	9.1	19.1	715	14.6	23.4	794	154.2	35.6	1122	110.8	23.7	9
1000	9.1	19.2	759	14.1	24.2	870	154.1	36.4	1239	110.8	23.8	9
1500	9.0	19.5	937	14.3	25.0	1015	153.2	39.7	1848	114.8	26.4	16
2000	9.0	19.8	1120	15.0	25.6	1159	150.8	41.1	2346	116.0	34.6	67

Columns as follows: r is the search radius in km, $\hat{S}_H$, the mean of the orientations of the maximum horizontal compressional stresses S_H given in degree, s_0 is the standard deviation of $\hat{S}_H$ given in degree (see Eq. (2) for definition) and N is the number of data records within the search radius r.

3.3. Variation of the statistical analysis parameter

The statistical analysis mainly depends on the choice of the number of data records N that are requested within the search radius and the threshold value for s_0. In Section 3.2 we presented the results for $N \geq 5$ and $s_0 < 25°$. With these values ~84,000 of the ~260,000 global 0.5° grid points returned values for the $\hat{S}_H$ orientation and r_{max} (Fig. 3). Changing N has no effect on the overall picture of these results. A smaller value for N is not justified from a statistical point of view and a higher N value would simply decrease the number of grid points for which values are returned. However, the impact of the chosen threshold value of s_0 is more critical at least for areas where the gradient of r_{max} is rather steep. This is seen e.g. in the western part of North America. Fig. 4 displays for this region the results with $N \geq 5$ and $s_0 < 20°$, 25° and 30°, respectively. The overall wave-length of the stress pattern remains, but in California and north of it, the colour flips from blue to red and vice versa when s_0 is increased or decreased by 5° (Fig. 4). In the first two rows of Table 4 the details of the statistical analysis reveal that s_0 is not decreasing steadily for decreasing search radii, but that several minima exist. This holds on for most of the values in Northern California. However, the change of s_0 does not affect at all the $\hat{S}_H$ orientation which documents the stability of the statistical approach. This is also true on a global scale and is also clearly seen in the data presented in Table 4. In most of the places s_0 is increasing steadily with decreasing search radius and the change of the $\hat{S}_H$ orientation as a function of r_{max} is always less than 15°.

Fig. 5 shows the impact of different s_0 values on the wave-length of the stress pattern for Europe. In comparison to California the changes are less drastic but more gradual. For a higher (lower) s_0 threshold value the number of grid points where results are returned increases (decrease) and areas of longer wave-lengths of the stress pattern expand (shrink). Again we observe that the rotation of the $\hat{S}_H$ orientation is small and rotations of ~20° are limited to a few sites (e.g. South Germany at 49.75°N, 9.75°E, Table 4). In contrast to previous findings of Müller et al. (1992) Western Europe exhibits short wave-lengths (<200 km) except for England, Wales, Ireland and in the area east of the Tornquist–Teissyre Zone that separates Western Europe from the East European Craton (Fig. 5). These findings are independent of the choice of N and the threshold value for s_0 (Fig. 5).

We also investigate if the result for the r_{max}-value estimation is changing when starting the search for r_{max} from $r = 100$ km upwards. Since for most of the grid points s_0 is decreasing steadily there is no significant change in the overall result (see examples in Table 4). However, in particular in California this is not true. Here the uneven distribution of the data record density leads to some areas where s_0 is not decreasing steadily but has local minima (second column of Table 4).

Furthermore, we checked whether higher or lower values for the search radius r change our results. Smaller r-values than used here have no impact on the general resulting stress pattern since most areas would not reach the minimum number of data records required (here $N = 5$) for smaller r. On a global scale $r = 50$ km would result only in ~350 additional grid points and has no impact on the wave-length of the stress pattern or the $\hat{S}_H$ orientation. Similar arguments hold on for higher search radii as the ones used in this analysis. For $r = 2000$ km the s_0-values increase in general above our chosen threshold s_0-value of 25° (Table 4).

4. Discussion and conclusions

The WSM database has been extensively expanded in the last 16 years, increasing from ~7700 data records in 1992 to 21,750 data records in 2008. However, it is important to note that the increase and improvements to the WSM database have not simply been due to addition of new data. The advances in stress determination techniques, new findings, and a better awareness of the reliability of stress indicators have also resulted in a large amount of data records from the original WSM 1992 database being removed or downgraded. For example the WSM 1992 database contained numerous indicators that are now classified as PBE or had been unreliably interpreted using automatic breakout picking software. Furthermore, the entries in the database have now been individually scrutinised, revealing a number of data records from the WSM database release 1992 that were incorrectly located or quality-ranked (even under old ranking schemes). In addition, the WSM project underwent in the last decade a gradual change in the data compilation philosophy. In the beginning the WSM project was rather hypothesis driven in order to investigate the questions whether there is a correlation between the intraplate S_H orientation in the Earth's crust and the plate motion as well as to address the question if the plate boundary forces are the principal source of crustal stress in intraplate regions (Sbar and Sykes, 1973; Zoback et al., 1989; Zoback and Zoback, 1991). Nowadays the WSM compilation is data driven, i.e. all data that pass the WSM quality-ranking scheme are added to the database. This approach resulted in a WSM database that has an increasing percentage of data from plate boundary areas and sedimentary basins, both areas that are most likely not representative for the long wave-length intraplate stress pattern (Tingay et al., 2005a,b, 2006; Heidbach et al., 2007).

Using a dataset of 11,347 A–C quality data records our statistical wave-length analysis of the global stress pattern results in a mean S_H orientation on a global 0.5° grid. In contrast to this, Coblentz and Richardson (1995) used a statistical analysis with fixed 5°×5° bins based on 4537 A–C quality data records. Surprisingly, the mean S_H orientations of Coblentz and Richardson (1995) are remarkably similar to those of the analysis presented here. However, due to the greater spatial coverage our analysis also provides mean S_H

Fig. 5. Smoothed stress map of Europe for three different values of s_0; same legend as in Fig. 3A. In most areas of central Europe and the Mediterranean short wave-length of the stress pattern is prevailing, indicating that regional to local stress sources contribute significantly to the $\hat{S}_H$ orientation. Only in Great Britain, Ireland, offshore west and east of the Tornquist–Teissyre Zone, that marks the border to the East European craton, the stress pattern displays longer wave-length. In contrast to California (Fig. 4) an increase of s_0 results in a gradual and smooth change of the wave-lengths of the stress pattern. Again, the $\hat{S}_H$ orientation is almost unaffected by the change of s_0.

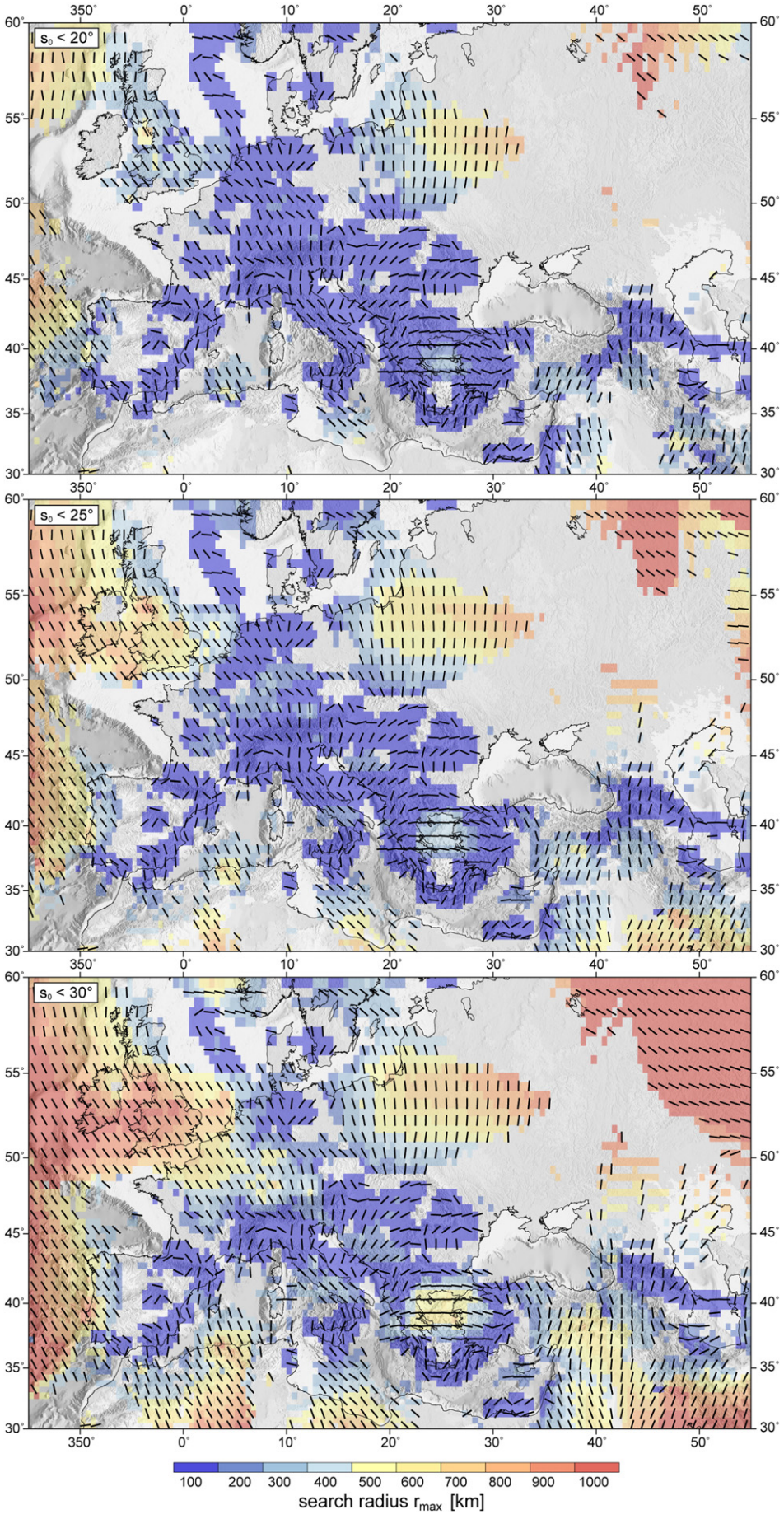
s0 < 20°
s0 < 25°
s0 < 30°
100 200 300 400 500 600 700 800 900 1000
search radius rmax [km]

orientations in places offshore Western Europe, Northern Africa, SE Asia, the western Pacific plate and Siberia. This analysis uses the same threshold value of the standard deviation $s_0<25°$ as was used in the study by Coblentz and Richardson (1995). However, the 5°×5° bins used in the Coblentz and Richardson (1995) study are quite large (approximately 550 km in N–S direction) and, as such, are much bigger than the adequate search radius observed in many regions herein. Indeed, our analysis of the stress patterns of western Europe, Alaska and the Aleutians, the southern Rocky Mountains, Scandinavia, most of the Himalayas, and Indonesia reveals shorter wave-length stress patterns, in the order of less than 200 km, that would not be detectable in the Coblentz and Richardson (1995) analysis.

The earlier visual and statistical analyses and interpretations (Müller et al., 1992; Zoback, 1992; Coblentz and Richardson, 1995) led to the conclusion that consistent S_H orientations exist across broad regions and that these orientations are the result from far-field plate boundary forces that are transmitted throughout the intraplate region. From the shorter wave-lengths of the stress pattern resulting from our study we conclude that the plate boundary forces either act over shorter distances or that local and regional stress sources are in the order of the magnitudes of the plate boundary forces. However, we cannot rule out that local high density of stress data records from sedimentary basins and the increasing number of data records that come from focal mechanisms near plate boundaries distort the long wave-length stress pattern. Thus, from our findings we cannot exclude that e.g. in Europe a long wave-length stress pattern is still prevailing at greater depth in the intraplate regions.

Regardless of these uncertainties our analysis estimates for the first time a global dataset of the mean S_H orientation on a 0.5° grid based on a sound statistical analysis. The tests on the statistical parameter showed that the results of the mean S_H orientations are robust. Thus, we provide this dataset and regular updates on the WSM project website (http://www.world-stress-map.org). Instead of using a single constant smoothing radius for the whole region of interest, which is often not justified, our smoothed S_H orientations can serve as a first-order guide of the stress pattern that takes into account its regional and local variability.

Acknowledgements

The World Stress Map project is a collaborative project that would not be possible without the effort of many scientists worldwide. We are indebted to numerous individual researchers and working groups all over the world for providing stress data. The authors are particularly grateful for major contributions for this WSM database release 2008 from Rosalind King, Marek Jarosinski, John Townend, Cecilia Guzman, Rima Chatterjee, Marcel Thielmann, Tobias Hergert, and Katrin Plenkers. We thank Friedemann Wenzel, Karl Fuchs, and the World Stress Map advisory board members Mark Zoback, Domenico Giardini, Onno Oncken, John Cook, Roy Gabrielsen, Egon Althaus, Chris Reigber, Markus Rothacher, and Helmut Kipphan for the long-term support. In particular we thank the two reviewers David Coblentz and Sören Gregerson for their critical review and comments that contributed significantly to the quality of this paper.

References

Angelier, J., 1979. Determination of the mean principal directions of stresses for a given fault population. Tectonophysics 56, T17–T26.
Bada, G., Cloetingh, S., Gerner, P., Horváth, F., 1998. Sources of recent tectonic stress in the Pannonian region: inferences from finite element modelling. Geophys. J. Int. 134, 87–101.
Barth, A., Wenzel, F., 2010. New constraints on the intraplate stress field of the Amurian plate deduced from low magnitude earthquake focal mechanisms. Tectonophysics 482, 160–169 (this issue).
Barth, A., Wenzel, F., Giardini, D., 2007. Frequency sensitive moment tensor inversion for light to moderate magnitude earthquakes in eastern Africa. Geophys. Res. Lett. 34 (L15302). doi:10.1029/2007GL030359.
Bell, J.S., 1996. In situ stresses in sedimentary rocks (part 2): applications of stress measurements. Geosci. Can. 23, 135–153.
Bird, P., 2003. An updated digital model for plate boundaries. Geochem. Geophys. Geosyst. 4 (3), 1027. doi:10.1029/2001GC000252.
Bird, P., Kong, X., 1994. Computer simulations of California tectonics confirm very low strength of major faults. Geol. Soc. Amer. Bull. 106, 159–174.
Bird, P., Ben-Avraham, Z., Schubert, G., Andreoli, M., Viola, G., 2006. Patterns of stress and strain-rate in southern Africa. J. Geophys. Res. 111 (B08402). doi:10.1029/2005JB003882.
Bott, M.H.P., 1959. The mechanics of oblique slip faulting. Geol. Mag. 96, 109–117.
Coblentz, D.D., Sandiford, M., 1994. Tectonic stresses in the African plate: constraints on the ambient lithospheric stress state. Geology 22, 831–834.
Coblentz, D., Richardson, R.M., 1995. Statistical trends in the intraplate stress field. J. Geophys. Res. 100 (B10), 20245–20255.
Coblentz, D., Zhou, S., Hillis, R.R., Richardson, R.M., Sandiford, M., 1998. Topography, boundary forces, and the Indo-Australian intraplate stress field. J. Geophys. Res. 103 (B1), 919–931.
Dyksterhuis, S., Albert, R.A., Müller, R.D., 2005. Finite-element modelling of contemporary and palaeointraplate stress using ABAQUS. Comput. Geotech. 31, 297–307.
Gephart, J.W., Forsyth, D.W., 1984. An improved method for determining the regional stress tensor using earthquake focal mechanism data: application to the San Fernando earthquake sequence. J. Geophys. Res. 89 (B11), 9305–9320.
Gregersen, S., 1992. Crustal stress regime in Fennoscandia from focal mechanisms. J. Geophys. Res. 97, 11821–11827.
Gregersen, S., Basham, P.W. (Eds.), 1989. Earthquakes at North Atlantic passive margins: neotectonics and postglacial rebound. Kluwer Academic Press. 716 pp.
Hardebeck, J.L., Michael, A., 2004. Stress orientations at intermediate angels to the San Andreas Fault, California. J. Geophys. Res. 109 (B11303). doi:10.1029/2004JB003239.
Heidbach, O., Barth, A., Connolly, P., Fuchs, F., Müller, B., Reinecker, J., Sperner, B., Tingay, M., Wenzel, F., 2004. Stress maps in a minute: the 2004 World Stress Map release. Eos Trans. 85 (49), 521–529.
Heidbach, O., Reinecker, J., Tingay, M., Müller, B., Sperner, B., Fuchs, K., Wenzel, F., 2007. Plate boundary forces are not enough: second- and third-order stress patterns highlighted in the World Stress Map database. Tectonics 26, TC6014. doi:10.1029/2007TC002133.
Heidbach, O., Tingay, M., Barth, A., Reinecker, J., Kurfeß, D., Müller, B., 2008. 2008. The World Stress Map database release. doi:10.1594/GFZ.WSM.Rel2008.
Heidbach, O., Tingay, M., Barth, A., Reinecker, J., Kurfeß, D. and Müller, B., 2009. The World Stress Map based on the database release 2008, equatorial scale 1:46,000,000, Commission for the Geological Map of the World, Paris. doi:10.1594/GFZ.WSM.Map2009.
Hickman, S.H., 1991. Stress in the lithosphere and strength of active faults. Rev. Geophys. 29, 759–775.
Hillis, R.R., Reynolds, S.D., 2000. The Australian Stress Map. J. Geol. Soc. 157, 915–921.
Kastrup, U., Zoback, M.L., Deichmann, N., Evans, K.F., Giardini, D., Michael, A.J., 2004. Stress field variations in the Swiss Alps and northern Alpine foreland derived from inversion of fault plane solutions. J. Geophys. Res. 109 (B01402). doi:10.1029/2003JB002550.
Ljunggren, C., Chang, Y., Janson, T., Christiansson, R., 2003. An overview of rock stress measurement methods. Int. J. Rock Mech. 40, 975–989.
Mardia, K.V., 1972. Statistics of Directional Data: Probability and Mathematical Statistics. Academic Press, London. 357 pp.
McKenzie, D., 1969. The relation between fault plane solutions for earthquakes and the directions of the principal stresses. Bull. Seismol. Soc. Am. 59 (2), 591–601.
Michael, J., 1984. Determination of stress from slip data: faults and folds. J. Geophys. Res. 89, 11517–11526.
Müller, B., Zoback, M.L., Fuchs, K., Mastin, L., Gregersen, S., Pavoni, N., Stephansson, O., Ljunggren, C., 1992. Regional patterns of tectonic stress in Europe. J. Geophys. Res. 97, 11783–11803.
Müller, B., Wehrle, V., Zeyen, H.J., Fuchs, K., 1997. Short-scale variations of tectonic regimes in the western European stress province north of the Alps and Pyrenees. Tectonophysics 275, 199–219.
Müller, B., Heidbach, O., Sperner, B., Negut, M., Buchmann, T., 2010. Attached or not attached - evidence from crustal stress observations for a weak coupling of the Vrancea slab in Romania. Tectonophysics 482, 139–149 (this issue).
Raleigh, C.B., Healy, J., Bredehoeft, J.D., 1972. Faulting and crustal stress at Rangley, Colorado. In: Heard, H.C. (Ed.), Flow and Fracture of Rocks. Geophys. Monogr. Ser. AGU, Washington, D.C., pp. 275–284.
Richardson, R.M., 1992. Ridge forces, absolute plate motions, and the intraplate stress field. J. Geophys. Res. 97, 11739–11748.
Rivera, L., Cisternas, A., 1990. Stress tensor and fault plane solutions for a population of earthquakes. Bull. Seismol. Soc. Am. 80, 600–614.
Sbar, M.L., Sykes, L.R., 1973. Contemporary compressive stress and seismicity in eastern North America, an example of intraplate tectonics. Geol. Soc. Amer. Bull. 84, 1861–1882.
Smith, W.H.F., Sandwell, D.T., 1997. Global sea floor topography from satellite altimetry and ship depth soundings. Science 277, 1956–1962.
Sperner, B., Müller, B., Heidbach, O., Delvaux, D., Reinecker, J., Fuchs, K., 2003. Tectonic stress in the Earth's crust: advances in the World Stress Map project. In: Nieuwland, D.A. (Ed.), New Insights in Structural Interpretation and Modelling. Special Publication. Geological Society, London, pp. 101–116.
Streit, J.E., 1997. Low frictional strength of upper crustal faults: a model. J. Geophys. Res. 102, 24619–24626.
Tingay, M., Müller, B., Reinecker, J., Heidbach, O., Wenzel, F., Fleckenstein, P., 2005a. The World Stress Map Project 'Present-day stress in sedimentary basins' initiative: building a valuable public resource to understand tectonic stress in the oil patch. Lead. Edge 24 (12), 1276–1282.

Tingay, M., Hillis, R.R., Morley, C.K., Swarbrick, E., Drake, S.J., 2005b. Present-day stress orientation in Brunei: a snapshot of 'prograding tectonic' in a Tertiary delta. J. Geol. Soc. Lond. 162, 39–49.
Tingay, M.R.P., Müller, B., Reinecker, J., Heidbach, O., 2006. State and origin of the present-day stress field in sedimentary basins: new results from the World Stress Map project. 41st U.S. Symposium on Rock Mechanics (USRMS): "50 years of Rock Mechanics — Landmarks and Future Challenges, Golden, Colorado, p. 14.
Townend, J., Zoback, M.D., 2004. Regional tectonic stress near the San Andreas Fault in central and southern California. Geophys. Res. Lett. 31 (L15S11). doi:10.1029/2003GL018918.
Townend, J., Zoback, M.D., 2006. Stress, strain, and mountain-building in central Japan. J. Geophys. Res. 111 (B03411). doi:10.1029/2005JB003759.
Zoback, M.L., 1992. First and second order patterns of stress in the lithosphere: the World Stress Map project. J. Geophys. Res. 97, 11703–11728.
Zoback, M., 2000. Strength of the San Andreas. Nature 405, 31–32.
Zoback, M.L., Zoback, M.D., 1980. State of stress in the conterminous United States. J. Geophys. Res. 85 (B11), 6113–6156.
Zoback, M.D., Healy, J., 1984. Friction, faulting and "in situ" stress. Ann. Geophys. 2 (6), 689–698.
Zoback, M.L., Zoback, M.D., 1989. Tectonic stress field of the conterminous United States. In: Pakiser, L.C., Mooney, W.D. (Eds.), Geophysical Framework of the Continental United States. Geol. Soc. Am. Mem., Boulder, Colorado, pp. 523–539.
Zoback, M.D., Zoback, M.L., 1991. Tectonic stress field of North America and relative plate motions. In: Slemmons, D.B., Engdahl, E.R., Zoback, M.D., Blackwell, D.D. (Eds.), Neotectonics of North America. InGeological Society of America, Boulder, Colorado, pp. 339–366.
Zoback, M.L., Mooney, W.D., 2003. Lithospheric bouyancy and continental intraplate stresses. Int. Geol. Rev. 45, 95–118.
Zoback, M.L., Zoback, M.D., Adams, J., Assumpção, M., Bell, S., Bergman, E.A., Blümling, P., Brereton, N.R., Denham, D., Ding, J., Fuchs, K., Gay, N., Gregersen, S., Gupta, H.K., Gvishiani, A., Jacob, K., Klein, R., Knoll, P., Magee, M., Mercier, J.L., Müller, B.C., Paquin, C., Rajendran, K., Stephansson, O., Suarez, G., Suter, M., Udías, A., Xu, Z.H., Zhizhin, M., 1989. Global patterns of tectonic stress. Nature 341, 291–298.